

Article

Microstructural and Fractographic Analysis of Plastically Deformed Al-Zn-Mg Alloy Subjected to Combined High-Cycle Bending-Torsion Fatigue

Aleksander Kowalski ^{1,*} , Wojciech Ozgowicz ², Wojciech Jurczak ³, Adam Grajcar ²,
Sonia Boczek ⁴ and Andrzej Kurek ⁵ 

¹ Institute of Non-Ferrous Metals, 5 Sowińskiego Street, 44-100 Gliwice, Poland

² Institute of Engineering Materials and Biomaterials, Silesian University of Technology, 18A Konarskiego Street, 44-100 Gliwice, Poland; wojciech.ozgowicz@tlen.pl (W.O.); adam.grajcar@polsl.pl (A.G.)

³ Faculty of Mechanical and Electrical Engineering, Polish Naval Academy, 69 Śmidowicza Street, 81-127 Gdynia, Poland; w.jurczak@amw.gdynia.pl

⁴ Light Metals Division, Institute of Non-Ferrous Metals, 19 Piłsudskiego Street, 32-050 Skawina, Poland; sboczek@imn.skawina.pl

⁵ Faculty of Mechanical Engineering, Opole University of Technology, 5 Mikołajczyka Street, 45-271 Opole, Poland; a.kurek@po.opole.pl

* Correspondence: aleksander.kowalski@imn.gliwice.pl; Tel.: +48-32-2380-232

Received: 7 June 2018; Accepted: 25 June 2018; Published: 26 June 2018



Abstract: The present manuscript aims to determine the effect of various deformation levels during low-temperature thermo-mechanical treatment (LTTT) on the microstructure and fatigue strength of Zr-microalloyed Al-Zn-Mg alloy. The fatigue strength of the alloy was studied in high-cycle bending-torsion tests. The determination of the influence of plastic deformation level during LTTT on the microstructure was based on transmission electron microscopy (TEM) observations. The analysis of fracture after the fatigue tests was performed based on fractographic images using scanning electron microscopy (SEM). It was found that the major factor affecting the microstructure of the alloy, and determining the nature of fatigue fracture, is the strain level applied during LTTT.

Keywords: aluminium alloy; 7003 alloy; fatigue strength; thermo-mechanical treatment; TEM; fractography

1. Introduction

Al-Zn-Mg alloys belong to a group of aluminium alloys which are particularly susceptible to low- and high-temperature thermo-mechanical treatments (HTTT). They are characterized by high stacking fault energy (SFE), which facilitates the occurrence of the polygonization process. Thermo-mechanical treatment uses plastic deformation of metals and enables their strengthening, mainly by increasing the density of lattice defects and phase transition processes, with the appropriate formation of microstructure, in technological operations. A low-temperature variation of the treatment, so called LTTT, is a method of thermo-mechanical processing often used for precipitation-strengthened aluminium alloys. It ensures obtaining high mechanical and fatigue properties of alloys while maintaining optimal plastic properties [1,2].

Despite a relatively large number of publications dealing with the impact of heat treatment and thermo-mechanical processing on the microstructure and mechanical properties of 7000 series alloys [3–7], there are relatively few studying the fatigue strength of these alloys. Moreover, publications on this matter focus mainly on the alloys containing Cu. For example, Gürbüz et al. [8] took up the issue of fatigue crack propagation of the 7475 alloy in underaged, peakaged, and overaged

states. An initiation of fatigue cracks and their development during high tensile fatigue loads in the 7075-T651 alloy were analyzed in [9]. In turn, Das et al. [10] investigated fatigue properties of this alloy rolled at cryogenic temperatures. Even though the alloys of this series are characterized by the highest strength indexes, their application for marine equipment and machines is limited. This is due to the difficulties encountered during welding and relatively low corrosion resistance in marine environment. Moreover, literature on the aspects of fatigue strength of 7000 series alloys are usually narrowed to cyclic tensile-compressive loads. Jo et al. [11] and Park et al. [12] investigated the effect of Mn addition to the Al-Zn-Mg alloy on the formation of dispersive particles, affecting the resistance of the alloys to fatigue cracking during cyclic tension-compression. Similarly, Deng et al. [13] studied strength properties of friction-welded joints in the 7050 alloy in tension-compression fatigue tests. Sporadically the results of fatigue bending, torsion, or tension with torsion have been also presented [14,15]. This work is focused on fractographic aspects of the fatigue of the AlZn6Mg0.8Zr alloy. Moreover, there are few papers dealing with a synergistic effect of bending-torsional loads on the fatigue strength of 7000 series aluminium alloys without the Cu addition.

2. Materials and Methods

2.1. Materials

A commercial sheet of aluminum 7003 alloy was investigated. The chemical composition of the used material is shown in Table 1. Low-temperature thermo-mechanical treatment was performed according to the scheme in Figure 1. Three major sets of the tests were performed. The solution heat treatment at 500 °C with 1 h holding, followed by water quenching, was treated as a reference state before the cold working. The cold rolling with a different reduction (10% and 30%) was applied to cause different deformation levels before the alloys were strain-aged. The strain ageing for 12 h at a temperature of 150 °C was the last heat treatment step.

Table 1. Chemical composition of the investigated alloy.

Elements	Zn	Mg	Mn	Fe	Cr	Si	Zr	Al
Mass fraction wt. %	6.13	0.74	0.29	0.19	0.17	0.12	0.08	Bal.



Figure 1. The scheme of the low-temperature thermo-mechanical treatment (LTTT).

2.2. Fatigue Behavior

The fatigue strength was determined using a MZGS-100 test-stand (Opole University of Technology, Faculty of Mechanical Engineering, Opole, Poland) [16]. The specimens were presented in Figure 2. They were subjected to the proportional combination of cyclic bending and torsion, the stresses being changed sinusoidally (stress ratio $R = -1$). The amplitude of bending and torsion moments was constant ($\sigma_{\max} = |\sigma_{\min}|$). The amplitude of torsional stress corresponded to half of the amplitude of the bending stress ($\tau_a = 1/2\sigma_a$).

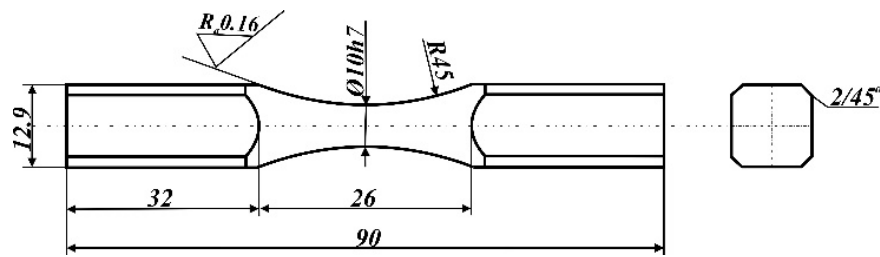


Figure 2. Test specimen used for fatigue strength tests.

To determine the fatigue strength of the alloy, a minimum of 17 tests were performed for each state of the material. In order to ensure high-cycle fatigue of specimens, the examinations were carried out at a diversified amplitude of stress. The failure criterion was used in two cases: (a) A total fracture of the specimen, or (b) when the test achieved 10^7 fatigue cycles. The fatigue characteristics of Basquin were presented in a diagram as the system $\log(\sigma_a) - \log(N_f)$. The solution heat-treated state was the basis to estimate the effect the LTTT parameters on the fatigue strength. The level of plastic deformation was the major parameter used in the comparative study of the fatigue strength. The fatigue tests of the AlZn6Mg0.8Zr alloy were performed in the range of fatigue cycles from approx. 2×10^4 to approx. 10^7 , and a normal stress amplitude from 112 MPa to 180 MPa.

In order to analyze the parallelism of the regression lines, the K parameter was used in the form:

$$K = \frac{m_{\sigma(1)}}{m_{\sigma(2)}} \quad (1)$$

where: K—the parameter determining the parallelism of regression lines, and $m_{\sigma(1)}$ and $m_{\sigma(2)}$ —the directional coefficients of compared regression lines.

2.3. Microstructure Observation

Transmission electron microscopy (TEM) investigations were carried out using a TECNAI G2 (FEI, Hillsboro, OR, USA) microscope. Thin foils of $\varnothing 3$ mm in diameter were prepared through the following steps: Cut out from the investigated alloy, ground using abrasive papers to the thickness of about 0.3 mm, and electrolytically polished using a Struers A2 reagent. An analysis of electron diffractions was carried out using an ELDYF computer program.

2.4. Fractography

In order to perform fractographic investigations, a scanning electron microscope (SEM) of the ZEISS SUPRA 25 type (Carl Zeiss AG, Jena, Germany) was applied with an electron device GEMINI (Carl, Zeiss AG, Jena, Germany) with a voltage of 20 kV. The specimens, after their decohesion in bending-torsion tests, were used. The main parameter of the LTTT used to compare the fatigue strength of the alloy was a strain level.

3. Results and Discussion

3.1. Fatigue Properties

The AlZn6Mg0.8Zr alloy subjected to LTTT with 10% deformation reveals a fatigue strength of 36,000 cycles at the maximum stress amplitude of 171 MPa, while at the minimum stress amplitude of 118 MPa, this strength is equal to 2,300,000 cycles (Figure 3). The 30% deformed alloy is characterized by a fatigue strength of 40,000 cycles and 820,000 cycles for the stress amplitudes equal to 174 MPa and 115 MPa, respectively. In the case of the solution heat treated specimens, the alloy under the stress amplitude of 180 MPa revealed a fatigue strength of 44,000 cycles, whereas at the stress amplitude of 112 MPa this was 2,350,000 cycles.

The alloy subjected to LTTT with 10% deformation loaded in a complex manner through the cyclic bending-torsion, for values of stress amplitude (σ_a) lower than approx. 150 MPa, showing a slightly higher fatigue strength when compared to the 30% deformed alloy (Figure 3). In the case of σ_a higher than approx. 150 MPa, a maximum fatigue strength was observed for 30% strain during the LTTT. The alloy solution heat-treated from 500 °C, loaded with complex cyclic stresses, shows the lowest temporary fatigue limit in the tested range of fatigue cycles. Regressions lines (with confidence intervals $\alpha = 0.05$) of the studied alloy in the solution heat-treated state and after LTTT with 10% and 30% reductions exhibit a parallelism coefficient K in the range of 1.0–1.2. The regression lines obtained after solution heat treatment and LTTT with 10% deformation are characterized by a maximum parallelism ($K = 1$). This indicates a similar fatigue strength under the analyzed conditions of cyclically variable loads. A comparative analysis of the results with the research conducted in the previous work of the authors [14] indicates that the fatigue strength of the alloy, subjected to complex bending with torsion, takes intermediate values between separate impacts of the oscillatory bending and double-sided torsion.

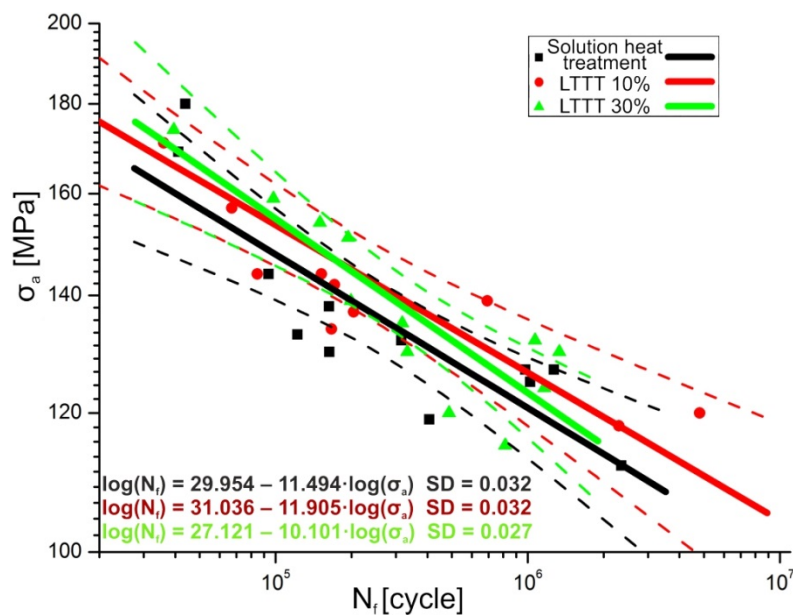


Figure 3. Basquin's diagram of regression lines with confidence intervals $\alpha = 0.05$ (dotted ines) for AlZn6Mg0.8Zr alloy subjected to the bending-torsion test after various stages of LTTT. SD—standard deviation.

3.2. Microstructure

Transmission electron microscopy of thin foils of the alloy subjected to 10% LTTT revealed the microstructure of α solution subgrains, with sizes in the range of 0.5–1 μm . Unevenly distributed, morphologically differentiated precipitates were found inside the subgrains (Figure 4a). In the vicinity of these boundaries, the presence of an indistinct precipitation-free zone was observed. This is a characteristic microstructural feature of precipitation-hardened Al-Zn-Mg alloys (Figure 4b). This has also been confirmed earlier by Kowalski et al. [17]. A gradual decay of the precipitation-free zone is caused by plastic deformation, resulting in concentration of dislocations being privileged areas for the precipitation of strengthening η -MgZn₂ phase. Obtained results are convergent with those presented by Cai et al. [18] and Huo et al. [19].

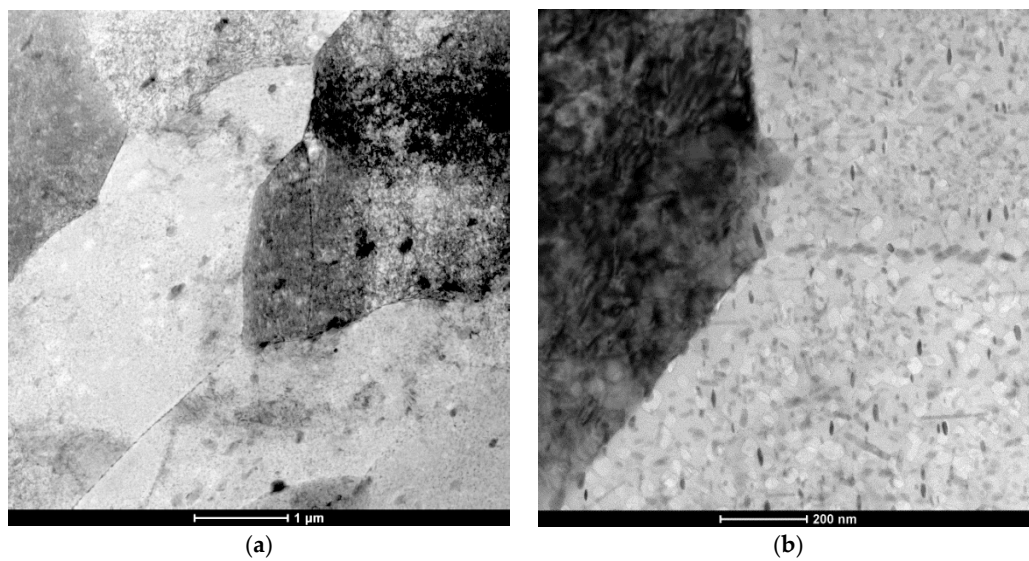


Figure 4. (a) Matrix of α solution with non-uniformly distributed precipitates; (b) Indistinct precipitation-free zone in the vicinity of boundaries of three grains.

A microstructure of the alloy subjected to LTTT with 30% reduction is characterized by a high density of dislocations inside the α matrix subgrains (Figure 5a). In the vicinity of the grain boundaries, the high quantity of fine, oval precipitates is visible, as well as individual particles with sizes exceeding approx. 100 nm (Figure 5b). No particular tendency to form precipitates as a continuous grid along the grain boundaries was observed. Moreover, the complete decay of precipitation-free zone was noted, which is in line with the previous considerations. Electron diffractions revealed reflexes from the α solution matrix (Al) and MgZn_2 phase, regardless of the deformation level during LTTT (Figure 6).

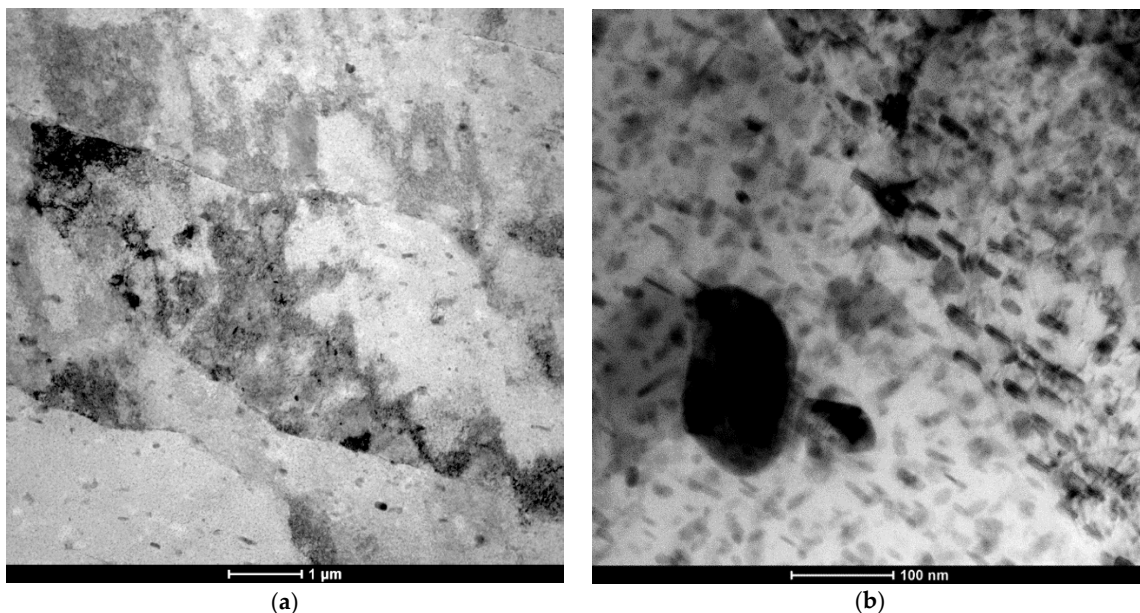


Figure 5. (a) Subgrains of α solution of the alloy with a high density of dislocations; (b) An irregular precipitate inside the α solution subgrain.

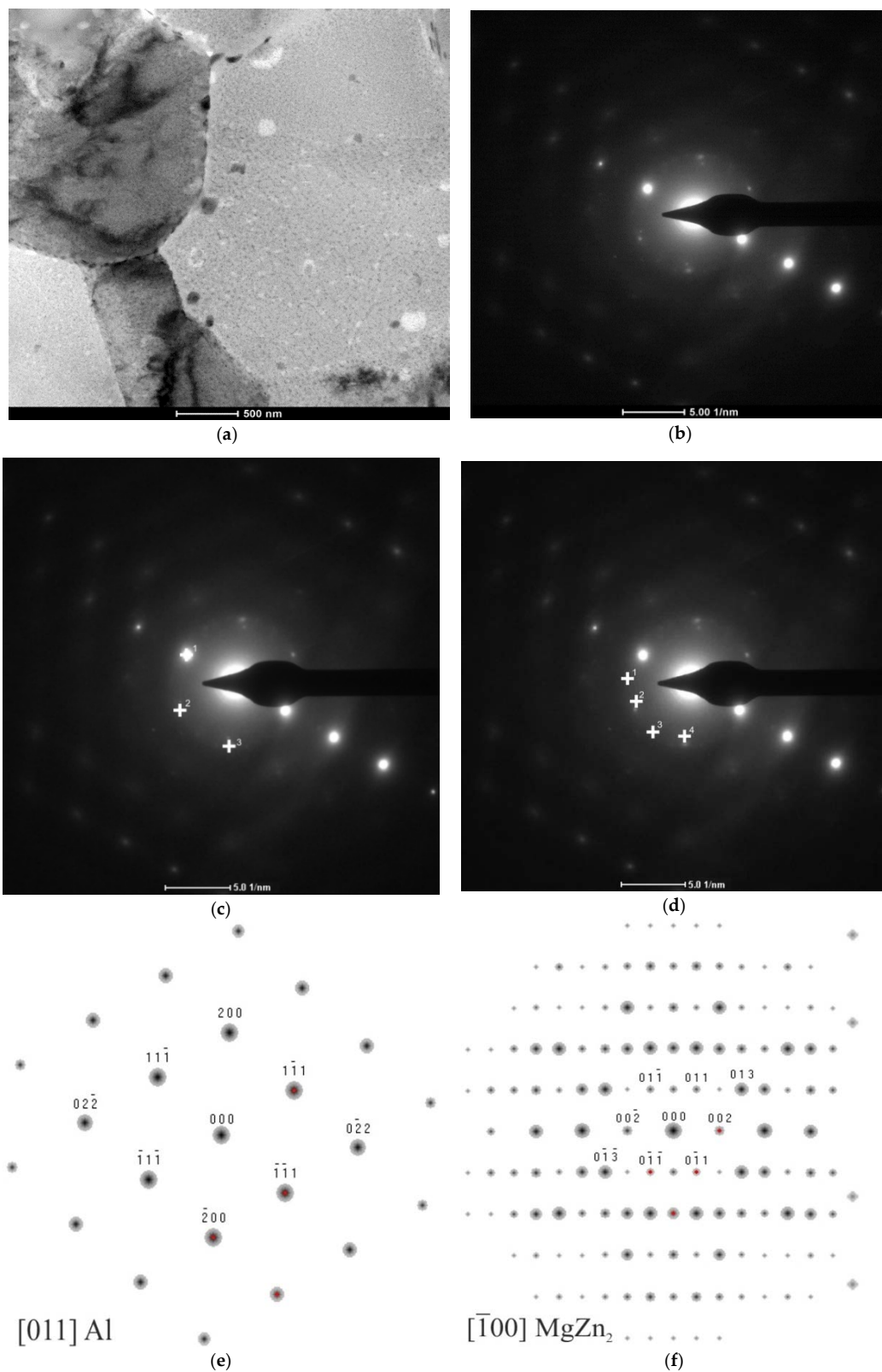


Figure 6. (a) Individual secondary precipitates inside the substructure of the 7003 alloy; (b) Electron diffraction; (c) Marked reflections of the α solution matrix; (d) Marked reflections of the $MgZn_2$ particle; (e) A solution of α phase matrix diffraction and (f) a solution of $MgZn_2$ phase diffraction.

3.3. Fractography

For specimens after the solution heat treatment, loaded in a complex manner under the bending-torsion conditions, clearly diversified heights of jogs of cleavage planes were observed on the fracture surfaces (Figure 7a). The secondary fatigue cracks and systems of jogs of cleavage planes twisted in relation to each other can be also noted. This indicates that the fracture during material fatigue occurred along many planes connected by the large jogs (Figure 7b,c). A particular location of these jogs may indicate a local direction change in the propagation of cracks, in the case of a complex state of fatigue stress (Figure 7d). The obtained results indicate that an increase in the fatigue crack occurs by connection of the successive smaller cracks initiated at the adjacent grain boundaries. This has been confirmed by Wang et al. [20], who observed that the propagation of the crack may be stopped when the front of the crack hits grain boundary, forming an angle of 90° or larger. The subsequent fatigue cycles cause an increase of a crack crevice width, and additionally initiate the formation of further cracks, especially at the grain boundaries, where the primary crack was stopped. In the next stage of fatigue, the main crack merges with those newly formed and the rate of crack propagation increases.

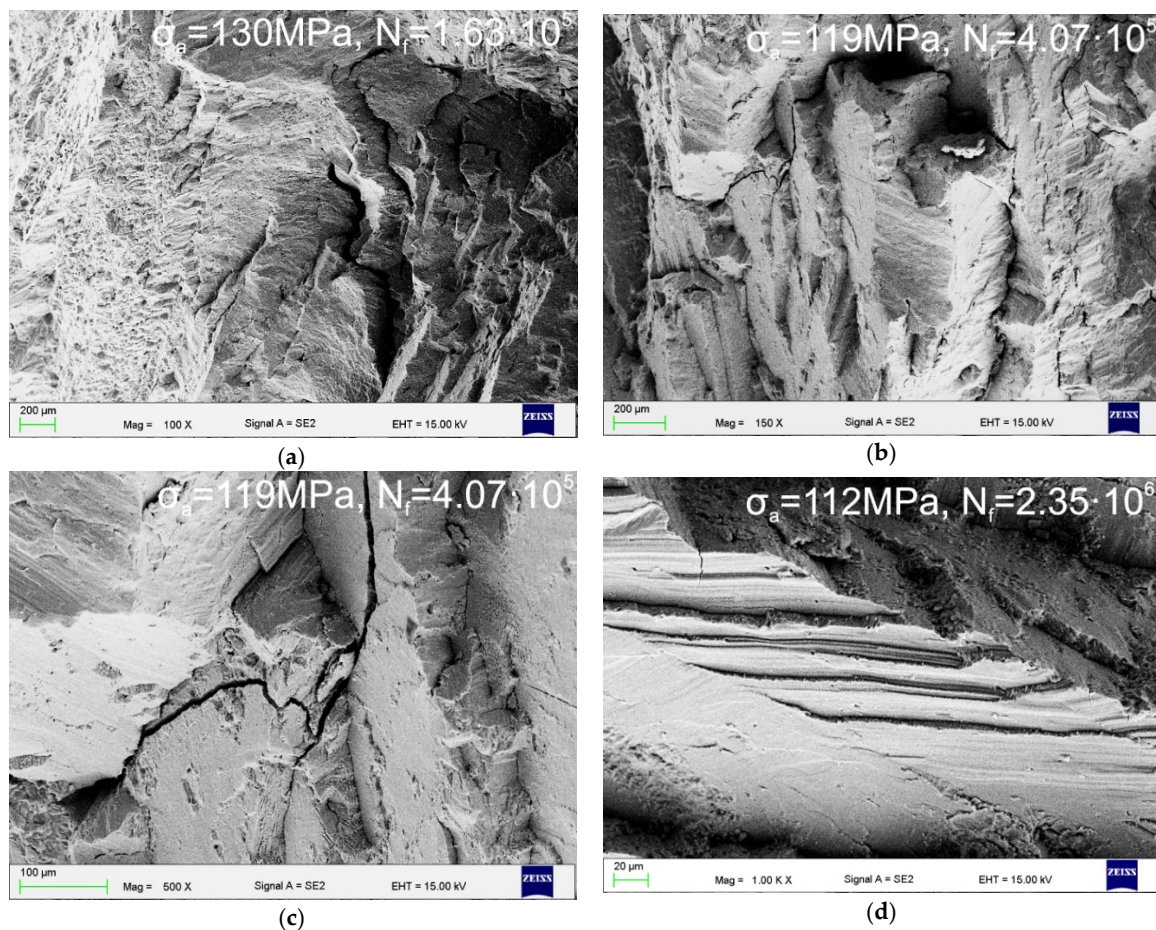


Figure 7. (a) Differently oriented systems of jogs of cleavage planes with various heights; (b) Inhomogeneous surfaces of jogs on fatigue fracture planes; (c) Systems of differently oriented cleavage planes; (d) Surfaces of fatigue cracking with cascade of jogs.

The samples after 10% LTTT, loaded in a complex way during bending with torsion, in the range of low-cycle stress amplitude, are of transcrystalline quasi-cleavage type (Figure 8a), with locally ductile areas (Figure 8b). In these areas, numerous craters of various diameters are visible. Intermetallic phases

are noted in these areas. Fracture areas of mixed character on the cleavage surfaces are noticeable (Figure 8c). For lower amplitudes of bending-torsional stresses in the range of a high number of cycles, the fractures are characterized by the presence of smooth jogs of transcrystalline-cleavage planes and tongue-like steps (Figure 8d).

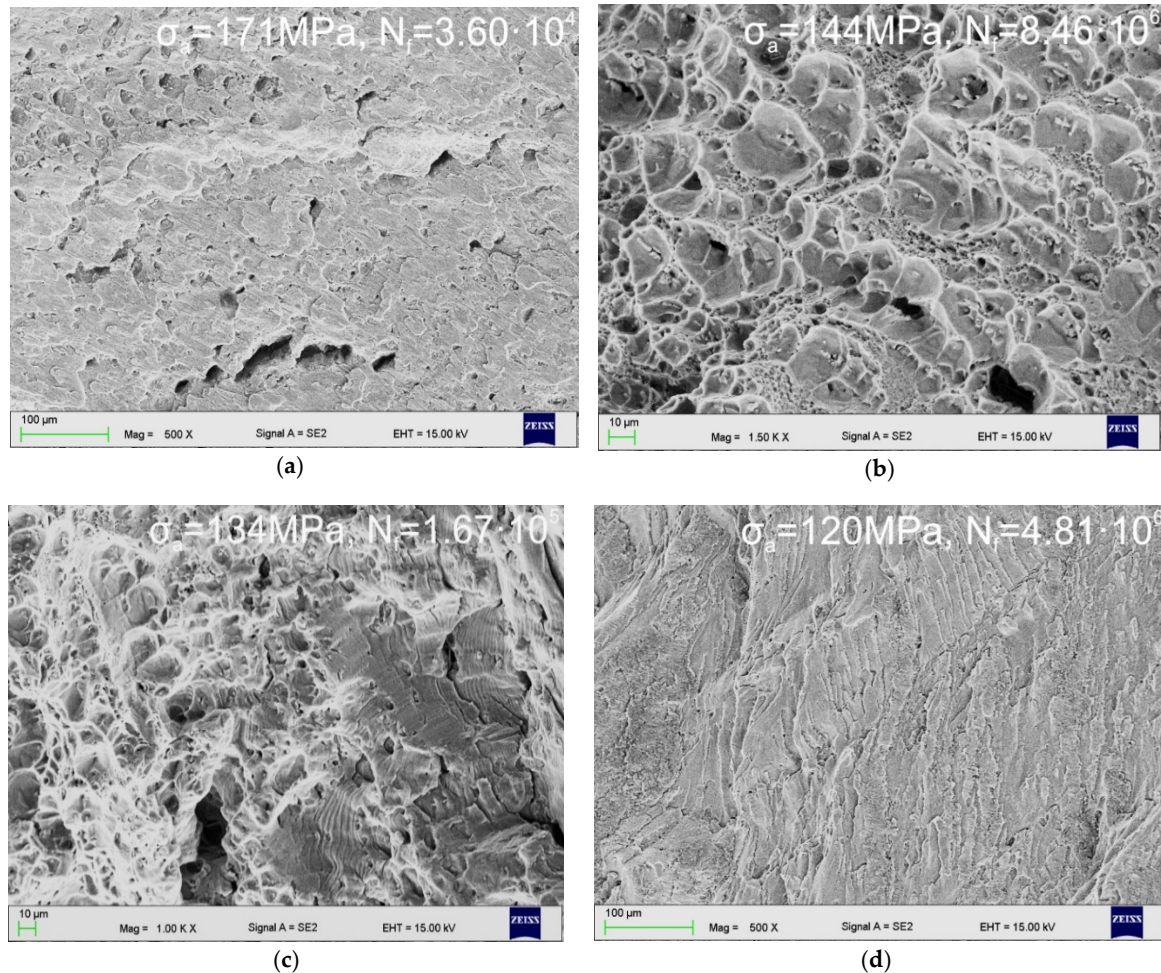


Figure 8. (a) Quasi-cleavage nature of fatigue fracture of the alloy; (b) Ductile fracture areas with precipitates on the bottom of cracks; (c) A mixed nature of scrap and fatigue striae on cleavage islands; (d) Cleavage planes tongue-like steps.

The alloy subjected to 30% LTTT, loaded in a complex manner under bending-torsion conditions ($\sigma_a = 174$ MPa and $\tau_a = 87$ MPa) in the low-cycle range, contains transcrystalline-quasi-ductile fracture with secondary cracks and flat islands of cleavage planes occurring locally (Figure 9a). A characteristic feature of scrap samples after bending with torsion with a stress amplitude of $\sigma_a = 159$ MPa and $\tau_a = 79$ MPa is the presence of irregularly shaped jogs, reflecting the secondary fatigue cracks (Figure 9b). The direction change of crack propagation is a common phenomenon in alloys containing dispersive particles of secondary phases, as reported by Jo, Park et al. [11,12]. This is caused by a crack front “avoiding” precipitation, leading to the curvature of the crack path. The high quantity of η -MgZn₂ phase particles present in the studied alloy ensures convenient conditions for the formation of extensive fatigue crack paths. However, complex loading conditions (causing activation of many cross-slip systems) favor such phenomena even more. In the case of the samples loaded with lower stresses ($\sigma_a = 135$ MPa, $\tau_a = 68$ MPa) in the high-cycle range, systems of jogs of cleavage planes are visible, with evidence of plastic deformation on the surface of jogs (Figure 9c). Loading the samples

with a stress amplitude of $\sigma_a = 124$ MPa and $\tau_a = 62$ MPa results in the disclosure of fracture areas, with a significant fraction of fatigue striae (Figure 9d).

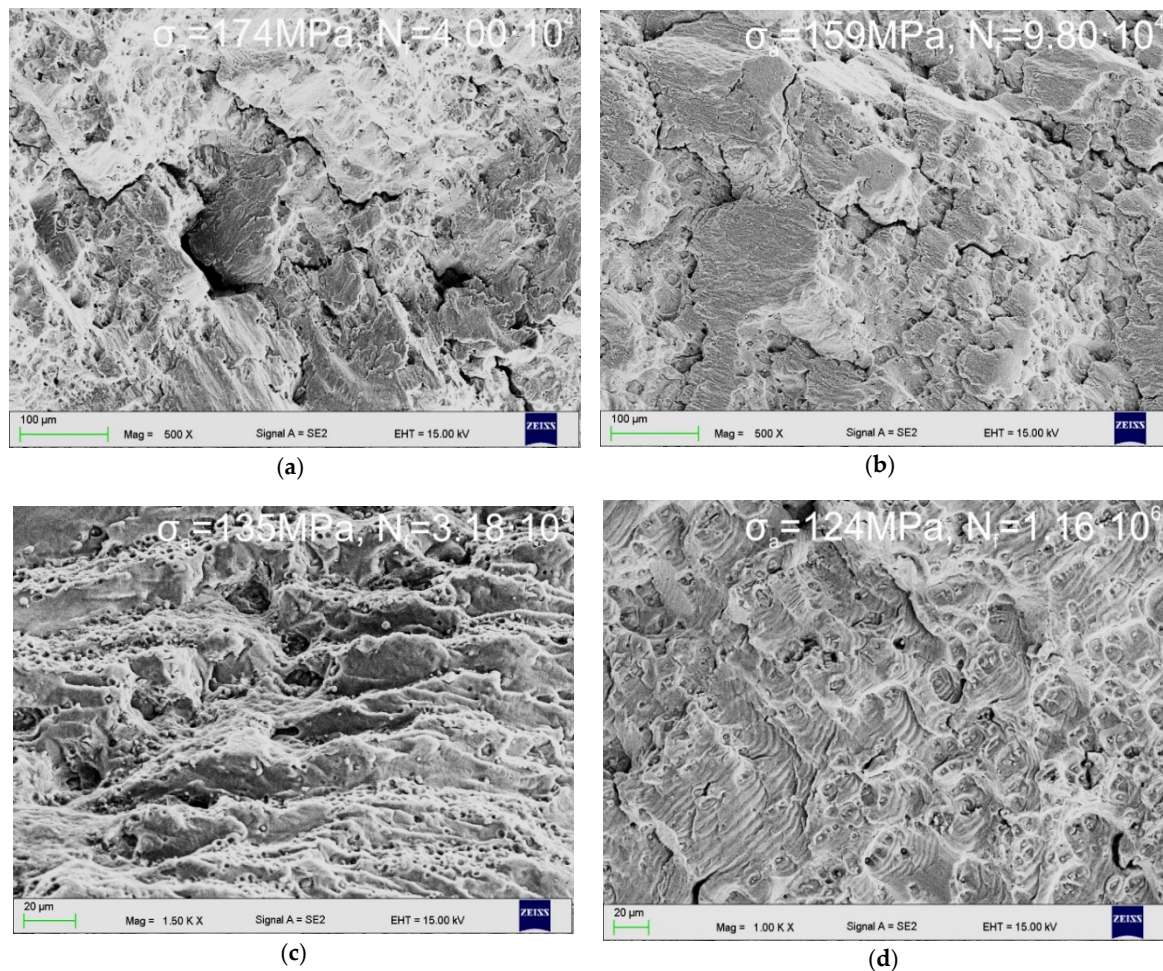


Figure 9. (a) Secondary cracks and islands of cleavage planes on the surface of the examined alloy; (b) Secondary cracks along the jogs of cleavage planes; (c) Traces of plastic deformation on the surfaces of jogs; (d) Systems of fatigue striae on the surface of the specimens.

4. Conclusions

The investigations on the microstructure and fatigue strength of the Al-Zn-Mg alloy processed through low-temperature thermo-mechanical treatment were a subject of the study. The fatigue strength of the alloy was verified under conditions of bending-torsion tests. The detailed analysis of the results of fatigue tests and metallographic observations of the AlZn6Mg0.8Zr alloy allowed the authors to formulate the following conclusions:

- Plastic deformation in the range of 10–30%, realized through cold rolling, leads to an increase of the density of privileged areas for homogeneous precipitation of the strengthening particles. It results in a more pronounced precipitation of η -MgZn₂ phase and a decay of precipitation-free zones in the vicinity of grain boundaries.
- The material condition after LTTT and the size of cyclic loads determine the portion of transcrystalline, quasi-cleavage, and ductile fracture. The increase in deformation level in the range of 10–30% results in an increase of the proportion of ductile fracture.
- Grain boundaries are the areas where the initiation of fatigue cracks is easy. Its propagation occurs mainly by the connection of successive cracks, which are formed on adjacent boundaries.

- The morphology and high dispersion of intermetallic η -MgZn₂ particles, and the activation of a significant quantity of cross slip systems, are the factors determining the formation of extensive crack paths under conditions of complex bending-torsion fatigue loads.

Author Contributions: A.K. (Aleksander Kowalski) and W.O. conceived and designed the experiments; A.K. (Aleksander Kowalski) performed fractographic observations, analyzed the data and wrote the paper; W.O. supervised the work; W.J. performed thermo-mechanical treatment and analyzed the results; A.G. analyzed the data and reviewed the paper; S.B. performed TEM experiments and analyzed the results; A.K. (Andrzej Kurek) performed fatigue tests and analyzed the results; All authors discussed the paper.

Funding: The financial support of The Silesian University of Technology is gratefully acknowledged.

Acknowledgments: The technical assistance of Wojciech Pakieła in SEM experiments is gratefully acknowledged.

Conflicts of Interest: The authors declare no conflict of interest.

References

1. Chemingui, M.; Khitouni, M.; Jozwiak, K.; Mesmacque, G.; Kolsi, A. Characterization of the mechanical properties changes in an Al-Zn-Mg alloy after a two-step ageing treatment at 70 °C and 135 °C. *Mater. Des.* **2010**, *31*, 3134–3139. [[CrossRef](#)]
2. Deschamps, A.; Livet, F.; Bréchet, Y. Influence of predeformation on ageing in an Al-Zn-Mg alloy—I. Microstructure evolution and mechanical properties. *Acta Mater.* **1998**, *27*, 281–292. [[CrossRef](#)]
3. Lü, X.; Guo, E.; Rometsch, P.; Wang, L. Effect of on-step and two-step homogenization treatments on distribution of Al₃Zr dispersoids in commercial AA7150 aluminium alloy. *Trans. Nonferr. Met. Soc. China* **2012**, *22*, 2645–2651. [[CrossRef](#)]
4. Thevenet, D.; Mliha-Touati, M.; Zeghloul, A. Characteristics of the propagation deformation bands associated with the Portevin-Le Chatelier effect in an Al-Zn-Mg-Cu alloy. *Mater. Sci. Eng. A* **2000**, *291*, 110–117. [[CrossRef](#)]
5. Khalid Rafi, H.; Janaki Ram, G.D.; Phanikumar, G.; Prasad Rao, K. Microstructure and tensile properties of friction welded aluminium alloy AA7075-T6. *Mater. Des.* **2010**, *31*, 2375–2380. [[CrossRef](#)]
6. Andreatta, F.; Terryn, H.; de Wit, J.H.W. Corrosion behavior of different tempers of AA7075 aluminium alloy. *Electrochim. Acta* **2004**, *49*, 2851–2862. [[CrossRef](#)]
7. Xiao, Y.P.; Pan, Q.L.; Li, W.B.; Liu, X.Y.; He, Y.B. Influence of retrogression and re-ageing treatment on corrosion behavior of an Al-Zn-Mg-Cu alloy. *Mater. Des.* **2011**, *32*, 2149–2156. [[CrossRef](#)]
8. Gürbüz, R.; Sarioğlu, F. Fatigue crack growth behavior in aluminium alloy 7475 under different aging conditions. *Mater. Sci. Technol.* **2001**, *17*, 1539–1543. [[CrossRef](#)]
9. Payne, J.; Welsh, G.; Christ, R.J., Jr.; Nardiello, J.; Papazian, J.M. Observations of fatigue crack initiation in 7075-T651. *Int. J. Fatigue* **2010**, *32*, 247–255. [[CrossRef](#)]
10. Das, P.; Jayaganthan, R.; Chowdhury, T.; Singh, I.V. Fatigue behaviour and crack growth rate of cryorolled Al 7075 alloy. *Mater. Sci. Eng. A* **2011**, *528*, 7124–7132. [[CrossRef](#)]
11. Jo, B.L.; Park, D.S.; Nam, S.W. Effect of Mn dispersoid on the fatigue crack propagation of Al-Zn-Mg alloys. *Metall. Mater. Trans.* **1996**, *27*, 490–493. [[CrossRef](#)]
12. Park, D.S.; Kong, B.O.; Nam, S.W. Effect of Mn-dispersoid on the low-cycle fatigue life of Al-Zn-Mg alloys. *Metall. Mater. Trans.* **1994**, *25*, 1547–1550. [[CrossRef](#)]
13. Deng, C.; Wang, H.; Gong, B.; Li, X.; Lei, Z. Effects of microstructural heterogeneity on very high cycle fatigue properties of 7050-T7451 aluminum alloy friction stir butt welds. *Int. J. Fatigue* **2016**, *83*, 100–108. [[CrossRef](#)]
14. Kowalski, A.; Ozgowicz, W.; Grajcar, A.; Lech-Grega, M.; Kurek, A. Microstructure and fatigue properties of AlZn6Mg0.8Zr alloy subjected to low-temperature thermomechanical processing. *Metals* **2017**, *7*, 488. [[CrossRef](#)]
15. Zhao, T.; Jiang, Y. Fatigue of 7075-T651 aluminum alloy. *Int. J. Fatigue* **2008**, *30*, 834–849. [[CrossRef](#)]
16. Kurek, A.; Wachowski, M.; Niesłony, A.; Płocinski, T.; Kurzydłowski, K.J. Fatigue tests and metallographic of explosively clad steel-titanium bimetal. *Arch. Metall. Mater.* **2014**, *59*, 1565–1570. [[CrossRef](#)]

17. Kowalski, A.; Ozigowicz, W.; Jurczak, W.; Grajcar, A.; Boczkal, S.; Żelechowski, J. Microstructure, mechanical properties and corrosion resistance of thermomechanically processed AlZn6Mg0.8Zr alloy. *Materials* **2018**, *11*, 570. [[CrossRef](#)] [[PubMed](#)]
18. Cai, Y.; Lang, Y.; Cao, L.; Zhang, J. Enhanced grain refinement in AA7050 Al alloy by deformation-induced precipitation. *Mater. Sci. Eng. A* **2012**, *549*, 100–104. [[CrossRef](#)]
19. Huo, W.T.; Shi, J.T.; Hou, L.G.; Zhang, J.S. An improved thermo-mechanical treatment of high-strength Al-Zn-Mg-Cu alloy for effective grain refinement and ductility modification. *J. Mater. Process. Technol.* **2017**, *239*, 303–3014. [[CrossRef](#)]
20. Wang, W.; Zhang, W.; Wang, H.; Fang, X.; Liang, X. Influence of grain boundary on the fatigue crack growth of 7050-T7451 aluminum alloy based on small time scale method. *Adv. Mater. Sci. Eng.* **2016**. [[CrossRef](#)]



© 2018 by the authors. Licensee MDPI, Basel, Switzerland. This article is an open access article distributed under the terms and conditions of the Creative Commons Attribution (CC BY) license (<http://creativecommons.org/licenses/by/4.0/>).